Journal of Radioanalytical and Nuclear Chemistry (2021) 328:669–678
https://doi.org/10.1007/s10967-021-07667-2

Biochar derived from *Salvadora persica* branches biomass as low-cost adsorbent for removal of uranium(VI) and thorium(IV) from water

Mohammad Albayari[1] · Mazen K. Nazal[2] · Fawwaz I. Khalili[3] · Norazzizi Nordin[1] · Rohana Adnan[1]

Received: 19 January 2021 / Accepted: 3 March 2021 / Published online: 21 March 2021

Abstract
In recent years, biochar based adsorbents have been given more attention for organic and inorganic pollutants removal. Therefore, in this study, a new low-cost biochar adsorbent derived from *Salvadora persica* branches (BSP) was prepared, characterized and investigated for removal of U(VI) and Th(IV) radioactive elements from water. The effects of batch adsorption conditions were studied. The maximum removal efficiencies are around 99% for each of U(VI) and Th(IV), with adsorption capacities 85.71 mg g^{-1} and 84.97 mg g^{-1} respectively. It has been found the adsorption process of U(VI) and Th(IV) is spontaneous, exothermic and follows pseudo-second-order kinetics.

Keywords Radioactive elements · Biomass adsorbent · Adsorption isotherms · Kinetics · Water treatment · Biochar

Introduction

Water treatment and removal of radioactive elements have been given high attention. Among these elements, uranium and thorium are found in rocks, soil and groundwater. Also, they are the main elements in the nuclear energy program. Although the concentrations of radioactive elements are low in the aquatic environment, the harmfulness and risk of these elements to the human, animals and plants are very high. Therefore, they are considered a serious threat to the ecosystem. Many biological studies reported that uranium and thorium cause dangerous diseases and they are carcinogen for kidney, liver, lung and pancreas [1, 2]. Therefore, effective removal of these radioactive ions from water is highly important. These facts have attracted the attention of many researchers and many methods were developed to remove U(VI) and Th(IV) ions from water, such as precipitation, ion exchange and extraction [3–6] and adsorption [7–11]. Among these methods, adsorption is one of the most widely used methods for the removal of metal ions from water. Adsorption method has several advantages such as it is a quite simple, efficient, relatively low cost, available, not producing sludge and capable of removing most forms of inorganic and organic material [9, 10]. The adsorption process depends mainly on the type of adsorbent. This gave the researchers more interest to investigate different adsorbents such as activated carbon, powdered activated carbon, activated alumina, charcoal, brick powder, activated sludge, zeolites and biomass [12–14]. Each of these materials has its advantages and disadvantages. However, looking for abundant, low-cost and highly efficient adsorbents still is required and of utmost importance. The biomass is renewable, abundantly available and considerably cheaper than the commercially available materials. The naturally available *Salvadora persica* plants biomass have many advantages. Their structure and components contain tannins, saponins, flavonoids, alkaloids and resin [15]. These components have different functional groups (e.g. carboxylic acid, hydroxyl, and amine) that may contribute to the final structure of a treated *Salvadora persica* as an adsorbent, and provide more efficient adsorption sites for U(VI) and Th(IV) ions. In recent years, the biochar based adsorbents have been given more attention for organic and inorganic pollutants removal. The biochar is a carbon rich material and it can be produced from several raw materials among them *Salvadora persica* branches. There are three preparation methods

✉ Mazen K. Nazal
mazennazal@kfupm.edu.sa

[1] School of Chemical Sciences, Universiti Sains Malaysia, 11800 Gelugor, Pulau Pinang, Malaysia

[2] Center for Environment and Water, Research Institute, King Fahd University of Petroleum and Minerals, Dhahran 31261, Saudi Arabia

[3] Department of Chemistry, Faculty of Science, The University of Jordan, Amman 11942, Jordan

of biochar (i.e. pyrolysis, hydrothermal carbonization and microwave carbonization). The pyrolysis method is the most common one and it is known as the thermal decomposition under oxygen-free conditions. The properties of biochar play a significant role in removal of contaminants, which is mostly governed by feedstock type and pyrolysis temperature. For instance, using pyrolysis temperature higher than 500 °C produces fully carbonized biochar which has more affinity for organic contaminants due to high hydrophobicity, microporosity, surface area and low dissolved organics. Oppositely, using pyrolysis temperature lower than 500 °C produces partially carbonized biochar which is more appropriate for inorganic contaminants removal due to the high content of dissolved organic carbon and oxygen-containing functional groups [16]. Considering the wide and high availability of feedstock, favorable chemical and physical properties and low-cost, the biochar shows promising performance to efficiently remove water organic and inorganic pollutants [17].

Therefore, a biochar derived from *Salvadora persica* branches biomass was prepared at temperature lower than 500 °C, and its adsorption performance for uranium and thorium ions from water was investigated. Effects of pH, adsorbent mass, and U(VI) and Th(IV) ions concentrations on the adsorption efficiency were studied. Also, the experimental results at equilibrium were fitted with the most frequently used adsorption isotherms and kinetics models. The thermodynamics parameters of U(VI) and Th(IV) ions adsorption were also calculated.

Experimental

Materials and methods

Salvadora persica branches were purchased from a local market in Saudi Arabia. The analytical grade chemicals were purchased as follows: thorium nitrate tetrahydrate from BDH, uranyl nitrate hexahydrate from (BDH) and Arsenazo(III) indicator from (Fluka), sodium nitrate, sodium hydroxide and hydrochloric acid from Sigma Aldrich, nitric acid (69%) from TEDIA. Deionized water was used to make up aqueous solutions and for washing all glassware. The concentrations of U(VI) and Th(IV) before and after the adsorption experiment were determined using a double-beam spectrophotometer (Spectroscan DU).

Preparation and characterization of adsorbent

The *Salvadora persica* branches were crushed and thoroughly washed then dried in an oven at 105 ± 0.3 °C. A biochar derived from *Salvadora persica* (BSP) was prepared through thermal pyrolysis of the dried branches, without any chemical treatment, inside a tube furnace (Lenton Furnace) at 400 °C with heating rate 10 °C/min for three hours, under a nitrogen atmosphere. The resulted biochar was washed thoroughly using deionized water and dried overnight in oven at room temperature. Without any further modification, the prepared biochar adsorbent was stored in glass vial later to be characterized and investigated for adsorptive removal of U(VI) and Th(IV) ions. The adsorbent surface' functional groups were characterized using Fourier-Transform Infrared (FTIR) (Nicolet 6700 Thermo Electron). The point of zero charge pH (pH_{pzc}) is generally described as the pH at which the net charge of absorbent's surface is equal to zero. In order to determine the pH_{pzc}, a 50 mg adsorbent were mixed with a 20 mL of 0.5 M of sodium nitrate solutions having different pH values ranging from 2 to 10 then the final pH values were measured using OAKTON PC2700 pH meter. The adsorbent surface morphology and elemental composition were characterized using Field Emission-Scanning Electron Microscope (FE-SEM) coupled with Energy Dispersive X-ray Spectroscopy (EDX) (Jeol 6700LV) instrument. The CHNO Elementar analyzer was used to determine the exact percentage of carbon, nitrogen and hydrogen elements in the prepared adsorbent. An automated nitrogen gas adsorption–desorption analyzer (Autosorb iQ Quantachrome USA) was used to determine the surface area (SA) and total pore volume (V) of the prepared adsorbent.

Batch adsorption experiments

The effect of batch adsorption conditions namely: pH of solution, weight of the prepared adsorbent, concentration of adsorbates ions, shaking time and adsorption temperature, on the removal of U(VI) and Th(IV) ions from water was studied. To study the effect of pH on the removal efficiency (Eq. 1), a 60 mg L^{-1} of each U(VI) and Th(IV) ions solutions having different pH (2–5) were prepared and mixed with a fixed adsorbent dosage (1 g L^{-1}) and agitated, in water bath shaker (Memmert GmbH Instrument, Germany) for 4 h at room temperature (25.0 ± 0.3 °C).

$$\text{Removal } \% = \frac{(C_o - C_e)}{C_o} \times 100\% \quad (1)$$

where C_o and C_e in mg L^{-1} are the adsorbate initial and equilibrium concentration respectively.

The effect of adsorbent dosage was studied by varying the added mass of adsorbent (10–200 mg) to a 50 mL solutions which have fixed pH (4.0), adsorbate concentration of 60 mg L^{-1} and temperature (25.0 ± 0.3 °C) then agitated for 4 h. The U(VI) and Th(IV) ions adsorption isotherms on the prepared adsorbent were investigated by studying the effect of their concentrations (i.e. 30, 40, 50, 60, 70 and 80 mg L^{-1}) on the adsorption capacity (q_e) (Eq. 2) of the

prepared adsorbent. A fixed adsorbent dose (1 g L^{-1}), solution pH (4.0) and shaking time (4 h) time were used and the most frequently adsorption isotherm models were tested and shown in Table 1.

$$q_e = \frac{V\left(C_o - C_e\right)}{m} \tag{2}$$

where V (L) and m (g) are the solution volume and adsorbent mass respectively.

For studying the effect of shaking time on the adsorption, a 1 g L^{-1} of BSP adsorbent dose was mixed with U(VI) and Th(IV) ions solutions having fixed concentration (60 mg L^{-1}) and pH (4.0) and kept for shaking at different time intervals (i.e. 15, 30, 45, 60, 120, 240, 480, 960, 1440 min) and fixed temperature (25.0 ± 0.3 °C). The obtained adsorption data were tested for different kinetics models (presented in Table 2).

In order to study the effect of temperature and obtaining the thermodynamics parameters of adsorption, a 60 mg L^{-1} concentration of U(VI) or Th(IV) were mixed with 1 g L^{-1} of BSP adsorbent for 4 h at a fixed pH (4.0) and different temperature (i.e. 25, 30, 35 and 40 ± 0.3 °C). The adsorption distribution coefficient (K_d) is calculated using the following equation:

$$K_d = \frac{q_e}{C_e} \tag{3}$$

The adsorption enthalpy (ΔH) and entropy (ΔS) are calculated from the slope and intercept of the van t'Hoff equation as follows:

$$\mathrm{Ln}\, K_d = \frac{\Delta S^\circ}{R} - \frac{\Delta H^\circ}{RT} \tag{4}$$

while the adsorption free energy (ΔG) is calculated using Eq. 5.

$$\Delta G^\circ = \Delta H - T\Delta S \tag{5}$$

Table 1 Linear forms of the most frequently used adsorption isotherms models

Isotherm	Linear equation	Plot	References
Langmuir	$\frac{C_e}{q_e} = \frac{1}{bQ_{max}} + \frac{C_e}{Q_{max}}$	$\frac{C_e}{q_e}$ vs . C_e	[18]
Freundlich	$\ln\left(q_e\right) = \ln\left(K_f\right) + \frac{1}{n}\ln\left(C_e\right)$	$\ln\left(q_e\right)$ vs. $\ln\left(C_e\right)$	[19]
Temkin	$q_e = \frac{RT}{b_T}\ln\left(A_T\right) + \frac{RT}{b_T}\ln\left(C_e\right)$	q_e vs. $\ln\left(C_e\right)$	[20]

Where Q_{max} (mg g^{-1}) is the maximum monolayer adsorption capacity in Langmuir model and b is the Langmuir constant. K_f (mg g^{-1}) (L $mg^{-1})^{1/n}$ and n (dimensionless) are the Freundlich model parameters. A_T (L g^{-1}) is the equilibrium binding constant in Temkin model related to the adsorption capacity, b_T (J mol^{-1}) is the Temkin constant related to the heat of adsorption, R (J K^{-1} mol^{-1}) is the ideal gas constant and T (K) is the temperature in Kelvin

Results and discussion

Characterization of BSP adsorbent

Figure 1 shows the FTIR spectrum of BSP adsorbent. The absorption stretching bands at around 3550 cm^{-1} and 3330 cm^{-1} indicate the presence of O–H and N–H related to alcohol and amine functional groups respectively. The medium peak at 2910 cm^{-1} is due to stretching of C–H associated with alkane. The strong stretching peaks at 1680 cm^{-1} and 1600 cm^{-1} corresponding to C=O and C=C in the conjugated ketone. Stretching peaks at 1110 cm^{-1} and 1010 cm^{-1} indicate the presence of C–O in ether and alcohol functional groups respectively [24]. Evidently, different functional groups are available which provide different potential adsorption sites for U(VI) and Th(IV) ions with. However, it is noticed that during biochar preparation the formation of the carboxylic acid is limited.

The biochar adsorbent's surface morphology is shown in Fig. 2a. It showed a complex irregular structure because of the decomposition and volatilization of *Salvadora persica* branches structural components (e.g. tannins, saponins, flavonoids and alkaloids). During the thermal pyrolysis of *Salvadora persica* at 400 °C, the volatile matter flows from the *Salvadora persica* branches structural components very fast in a short period which leads to splitting and shrinking of the surface as a result, formation of pores with different

Table 2 Linear equations of the tested kinetics models

Kinetics model	Linear equation	Plot	References
Pseudo-first order (PFO)	$\ln\left(q_e - q_t\right) = \ln\left(q_e\right) - k_1 t$	$\ln\left(q_e - q_e\right)$ vs. t	[21]
Pseudo-second order (PSO)	$\frac{t}{q_t} = \frac{1}{q_e^2 k_2} + \frac{t}{q_e}$	$\frac{t}{q_t}$ vs. t	[22]
Intra-particle diffusion	$q_t = k_{id} t^{0.5} + C$	q_t vs. $t^{0.5}$	[23]

where q_t in mg g^{-1} is the adsorption capacity at certain time t in minutes, k_1 (min^{-1}) and k_2 (g mg^{-1} min^{-1}) are the rate constants in pseudo-first order and pseudo-second order kinetics models respectively. k_{id} (mg g^{-1} $min^{-0.5}$) is the intra-particle diffusion rate constant, and C (mg g^{-1}) is a constant related to the thickness of boundary layer in Weber–Moris equation [23]

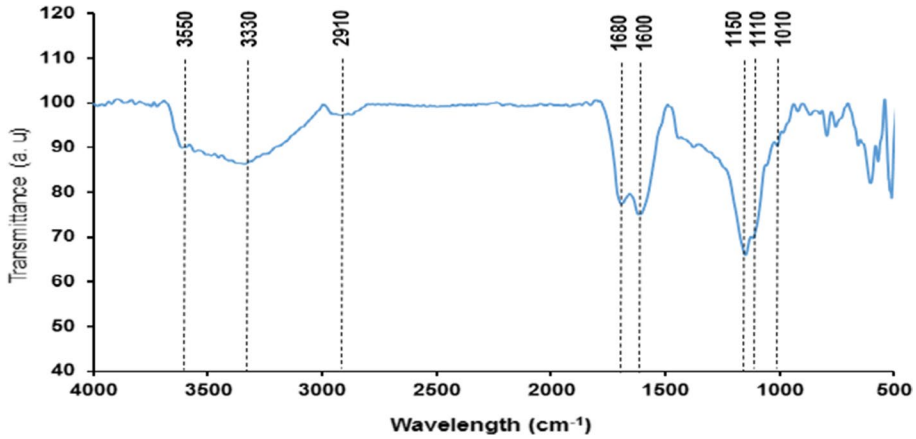

Fig. 1 FTIR spectrum of Biochar *Salvadora persica* (BSP) adsorbent

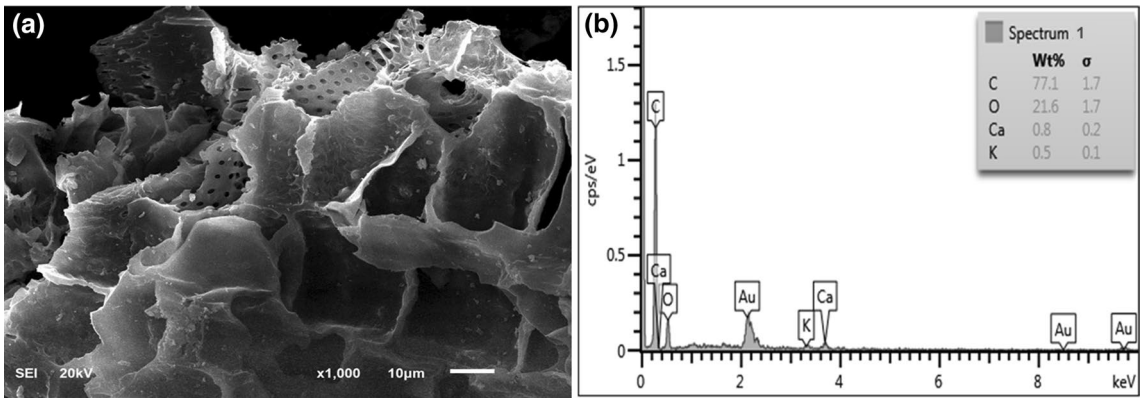

Fig. 2 **a** FE-SEM image of BSP adsorbent surface and **b** EDX spectrum

sizes and shapes [25]. This is in agreement with the assumption that morphological changes in the original materials occurred to some extent during the biochar formation reactions [26]. The elemental analysis results obtained by the CHNO analyzer show that the prepared adsorbent has 74.24% of carbon, 4.04% of hydrogen, 0.59% of nitrogen and 21.13% of oxygen. The percentages of carbon and oxygen elements are very close to the results of EDX (shown in Fig. 2b). It has been found that carbon and oxygen are the major elements of the adsorbent while some mineral fractions of Ca (0.8%) and K (0.5%) were also detected. This indicates that the carbon and oxygen are the skeleton of the BSP adsorbent which may come from the organic compounds having oxygen-containing functional groups such as hydroxyl, ether and ketone.

For further characterization, the proximate and surface area analyses are conducted. It has been found that BSP adsorbent has 5.18% of moisture (M), 20.12% of volatile matter (VM), 70.01% of fixed carbon (FC) and 5.36% of ash. The surface area, total pore volume and pore radius are 9.05 $m^2\ g^{-1}$, 0.011 mL g^{-1} and 8.9 Å respectively.

pH effect

The pH of solution influences the metals speciation as well as the active adsorption sites available on the surface of the adsorbents. In the effect of pH study and as shown in Fig. 3, it has been found that the removal percentages of U(VI) and Th(IV) increase and reach the maximum at pH 3.0. This may be attributed to the change of the adsorbent surface charge, from positive to negative, at pH higher than the adsorbent pH_{pzc} (2.79). This leads to increase the electrostatic interaction between U(VI) and Th(IV) ions and the negatively charged adsorbent surface. Moreover, at pH less than 3, the concentration of H^+ ion is high and these ions compete with U(VI) and Th(IV) ions for the interacting with the active adsorption sites on the surface of adsorbent [27]. Also, at pH between 3 and 4, the extractable species of U(VI) (e.g. UO_2^{2+}, $(UO_2(OH)^+$ and $(UO_2)_2(OH)_2^{2+}$)) and Th(IV) (e.g. Th^{4+}, $Th(OH)^{3+}$, $Th(OH)_2^{2+}$ and $Th(OH)_3^+$) are formed and dominant [28, 29]. Hence, a pH equal 4.0 ± 0.1 was chosen later in the adsorption experiments.

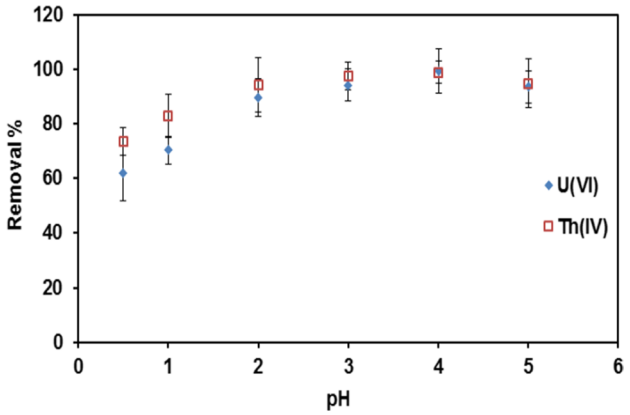

Fig. 3 Effect of pH on the percentage removal of U(VI) (60 µg mL^{-1}) and Th(IV) (60 µg mL^{-1}) using BSP adsorbent (1 g L^{-1}) at 25 ± 0.3 °C and contact time 240 min

Effect of adsorbent dose

Figure 4 shows the effect of the loaded BSP adsorbent dose on the removal efficiency of U(VI) and Th(IV) ions. It has been found that the maximum removal efficiency of 99% is obtained using 1 g L^{-1} of adsorbent. This is attributed to the increase of active adsorption sites by increasing the adsorbent mass.

Effect of initial concentration

Figure 5 shows the concave to the axis adsorption isotherms of U(VI) and Th(IV) which match type I adsorption isotherm. This indicates the adsorption sites distributed homogenously on the surface of adsorbent [30]. Different isotherm models were tested for U(VI) and Th(IV) adsorption onto BSP adsorbent. The plots of the linear forms of the tested adsorption isotherm models are presented in Fig. 6.

The models' parameters for U(VI) and Th(IV) adsorption onto BSP are summarized in Table 3. These parameters

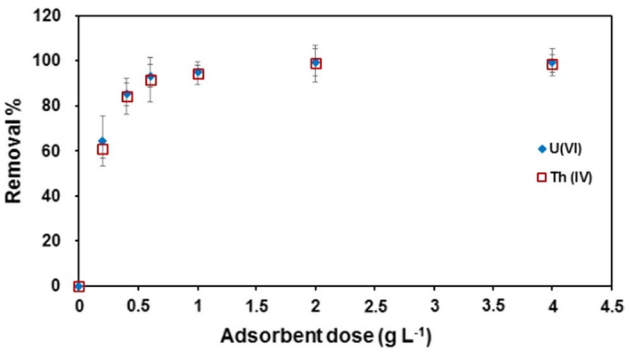

Fig. 4 Effect of BSP adsorbent dose on the removal of U(VI) (60 mg L^{-1}) and Th(IV) (60 mg L^{-1}) at 25 ± 0.3 °C and contact time 240 min

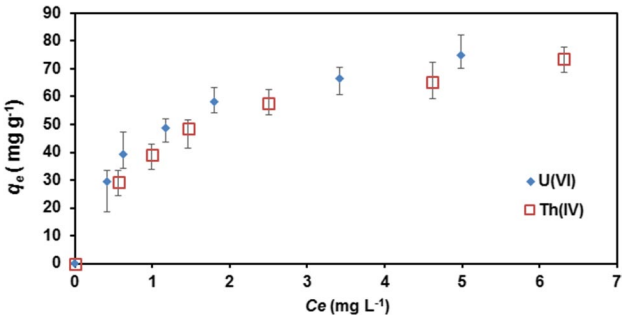

Fig. 5 Adsorption isotherms curves of U(VI) and Th(IV) onto BSP adsorbent at 25 ± 0.3 °C and contact time 240 min

were calculated from the slope and the intercept of the corresponding adsorption isotherm model linear form. It has been found that Langmuir and Temkin isotherms are the best fit to the experimental adsorption results of U(VI) and Th(IV) ions with squared correlation coefficients (R^2) higher than 0.99. As a result, we are expecting that the BSP adsorbent's surface is almost homogenous and the chemisorption mechanism is predominant. The obtained separation factor (R_L) from Langmuir constant (b) is calculated using Eq. 6. The value of R_L, between zero and one, shows the favorability of U(VI) and Th(IV) ions adsorption. The maximum monolayer adsorption capacity of BSP for U(VI) and Th(IV) ions are 85.71 and 84.97 mg g^{-1}. Positive b_T value obtained from Temkin model indicates that the adsorption process is exothermic. Therefore, the proposed interactions mechanism between these ions and BSP surface mostly involve an ion-exchange interaction. In Freundlich, the n and K_f values which are higher than 1 indicate that the adsorption of U(VI) and Th(IV) ions onto BSP is favorable. The higher magnitude of these values corresponds to higher adsorption capacity [31].

$$R_L = {}^{1}/_{(1 + bC_o)} \quad (6)$$

In Table 4, the maximum adsorption capacity of the prepared adsorbent in this study for U(VI) and Th(IV) ions are compared with other published results. It has been found that the BSP has high adsorption capacity and it is comparable with many adsorbents reported in the literature.

Effect of contact time and adsorption kinetics

The contact time is a vital parameter affecting on the removal efficiency. As shown in Fig. 7, the BSP removal efficiencies for U(VI) and Th(IV) increase rapidly in the first 1 h which is attributed to the maximum availability of unoccupied adsorption sites on the surface of adsorbent. Then they reach equilibrium within 2 h. Figure 8 shows the plots of the linearized kinetics models (i.e. PFO and PSO).

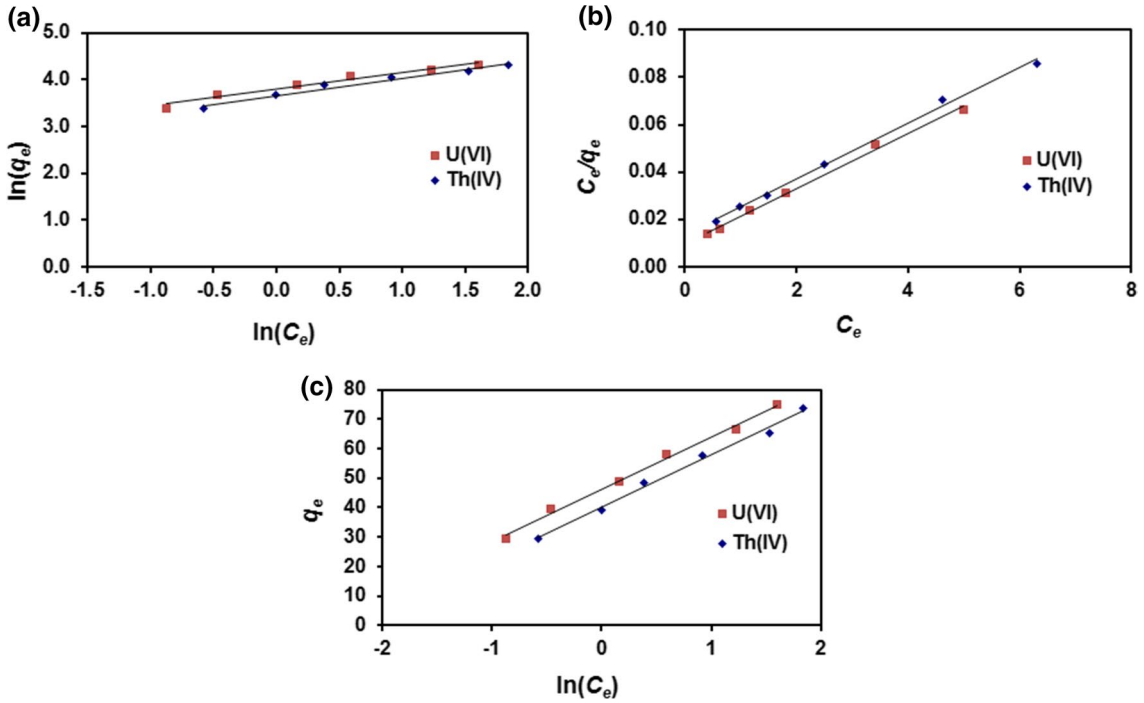

Fig. 6 Linear least squares fit of **a** Freundlich model, **b** Langmuir model and **c** Temkin model for U(VI) and Th(IV) adsorption onto BSP at 25 ± 0.3 °C

Table 3 Freundlich, Langmuir and Timken isotherms models parameters and correlation coefficient for U(VI) and Th(IV) adsorption on Biochar *Salvadora persica* branches adsorbent at 25 ± 0.3 °C

	U(VI)	Th(IV)
Freundlich		
K_f ((mg g^{-1}) (L mg^{-1})$^{1/n}$)	44.18	38.93
n	2.81	2.74
R^2	0.9675	0.9709
Langmuir		
Q_o (mg g^{-1})	85.71	84.97
b	1.21	0.87
R^2	0.9968	0.9961
R_L	0.014	0.019
Temkin		
AT (L g^{-1})	1.40	1.34
b_T (J mol^{-1})	137.14	135.91
R^2	0.9945	0.9931

The adsorption kinetics' parameters are calculated from the slope and the intercept of the corresponding linear plot and summarized in Table 5. The obtained squared correlation coefficients (R^2) are 1 and the q_e experimental ($q_{e\,exp.}$) and q_e calculated ($q_{e\,calc.}$) values are very close to each other in PSO for both ions. This clearly indicates the adsorption of U(VI) and Th(IV) onto BSP adsorbent follows the PSO kinetics, which is in role shows involvement of chemisorption in the rate-determining step in the adsorption mechanism [45].

For further investigation of adsorption mechanism and to know if U(VI) and Th(IV) adsorption is described as a diffusion-controlled process, the equilibrium adsorption data were fitted to the most widely applied intra-particle diffusion model described by Weber and Morris [23]. As shown in Fig. 9, plotting of q_t versus $t^{0.5}$ reveals two linear parts. This indicates that U(VI) and Th(IV) adsorption governed through two diffusion steps. The first step is fast and related to the external mass transfer of U(VI) and Th(IV) from the bulk solution to the available pores and adsorption sites on the surface of the adsorbent, while the second step arises from the pore diffusion and adsorption of these ions onto the adsorption sites which followed by the establishment of equilibrium. Moreover, the plots did not pass through the origin which indicates the intra-particle diffusion was not the only rate determining step [46, 47]. Table 6 summarizes the calculated intra-particle parameters.

Thermodynamics of adsorption

The adsorption enthalpy (ΔH) and entropy (ΔS) of U(VI) and Th(IV) are calculated from the slope and intercept of the van t'Hoff (Ln(K_d) vs. 1/T) (shown in Fig. 10). Table 7 summarizes the thermodynamics parameters for U(VI) and

Table 4 Comparison of the reported adsorption capacity of different adsorbents for U(VI) and Th(IV) at the studied pH

Adsorbent	pH	Q_{max} (mg g^{-1})	Reference
U(VI)			
Coffee residues	4.0	40.5	[11]
Lemon peel	8.0	24.39	[12]
Granular activated carbon modified with Nitric acid	5.0	23.81	[13]
Ethylenediamine-modified biomass of *Aspergillus niger*	5.0	4.31 (unmodified) 6.78 (modified)	[32]
Salvadora persica branches biomass	4.0	24.85	[11]
Biochar produced by pine needles hydrothermal carbonization	6.0	62.7	[33]
Ethyl acetate treated clay (TC)	4.5	38.91	[34]
Manganese oxide coated zeolite (MOCZ)	4.0	15.1	[35]
Silica gel	5.15	97.9	[36]
Hydroxyapatite coated activated carbon powder nanocomposite (HAP-AC)	–	3.83	[37]
Hydrazine-impregnated activated carbon	Highly Acidic	5.91	[38]
Biochar derived from *Salvadora persica* branches (BSP)	4.0	85.71	This work
Th(IV)			
Rice bran	−0.6	49.3	[39]
Wheat bran	−0.6	38.7	
Granular activated carbon modified with Nitric acid	5.5	36.23	[13]
Insolubilized humic acid originated from Ajloun	3.0	35.71	[40]
Duckweed pyrolytic biochar at 600 °C	2.7	71.7	[41]
Salvadora persica branches biomass	4.0	21.21	[11]
Activated biochar produced from *Opuntia ficusindica* cactus fibres	3.0	81	[42]
1-Amino-2-naphthol-4-sulphonic coupled chitosan (ANSC)	2.5	252.57	[43]
2-Thenoyltrifluoroacetone modified Santa Barbara amorphous silica (TTA-SBA-15)	4.0	36.10	[44]
Biochar derived from *Salvadora persica* branches (BSP)	4.0	84.97	This work

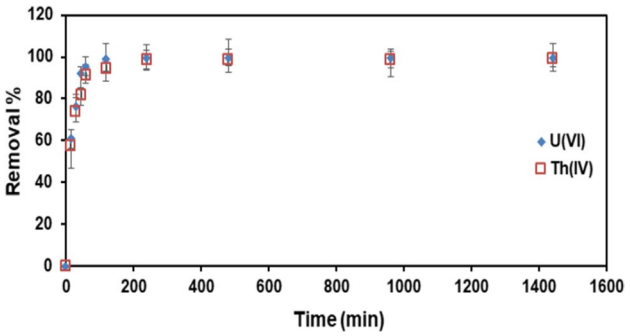

Fig. 7 Contact time effect on the removal efficiency of BSP for U(VI) and Th(IV) ions at 25 ± 0.3 °C. Concentration of each is 60 mg L^{-1}, adsorbent dosage concentration is 1 g L^{-1}

Th(IV) adsorption onto BSP adsorbent. It has been found that the free energy (ΔG) values are negative in the studied temperature range (25–40 ± 0.3). This indicates the adsorption process is spontaneous and thermodynamically favorable. Increasing the ΔG values with increasing the temperature and the negative values of ΔH for both ions indicate that the adsorption process is exothermic. In addition, the obtained values of ΔH, −218.17 kJ mol^{-1} and −240.17 kJ mol^{-1} for U(IV) and Th(IV) respectively, reveal that the chemical adsorption mechanism is predominant [48, 49]. The observed exothermic effect can be explained by the forces of interaction between the adsorbent and U(IV) and Th(IV), which are stronger than those existing in both adsorbent and U(IV) and Th(IV) alone, which means that it would prefer the product than reactant [50]. The small negative entropy values in the adsorption system in this study indicates that the randomness decreases at the adsorbate/adsorbent interface.

Mechanism of U(VI) and Th(IV) ions adsorption

The prepared adsorbent can remove uranium and thorium ions through chelation mechanism via the unpaired electrons at the nitrogen of amino groups and oxygen of hydroxyl and carbonyl groups on the adsorbent surface. Also, through an ionic interaction between the negatively charged functional groups and the U(VI) and Th(IV) cations.

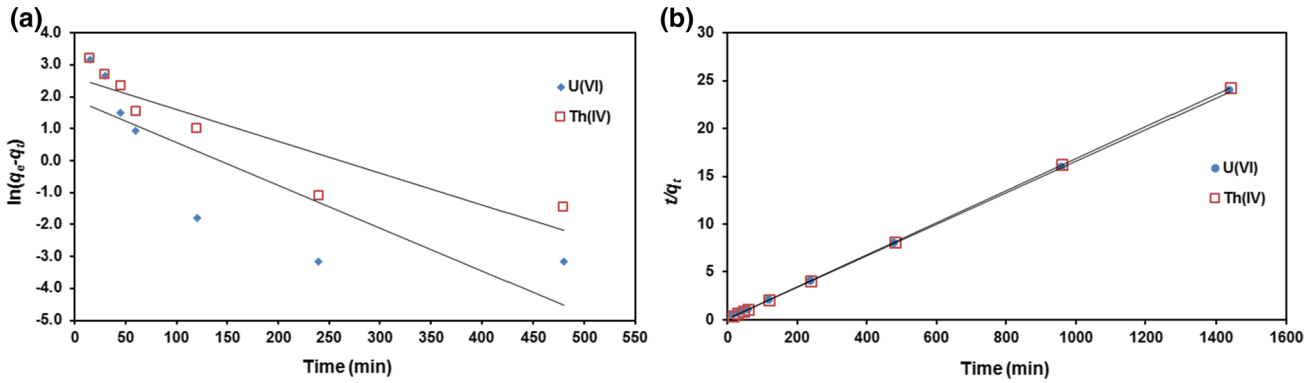

Fig. 8 Linear least square fit for **a** PFO and **b** PSO models for U(VI) and Th(IV) adsorption onto BSP adsorbent at 25 ± 0.3 °C

Table 5 PFO and PSO adsorption kinetics parameters for U(VI) and Th(IV) adsorption onto BSP adsorbent

Ion	$q_{e\,exp}$	$q_{e\,calc}$	k_1 (1 min^{-1})	R^2
PFO				
U(VI)	60.33	6.73	3.09×10^{-2}	0.6981
Th(IV)	59.48	13.30	2.28×10^{-2}	0.8300
	$q_{e\,exp}$	$q_{e\,calc}$	k_2 (g mg^{-1} min^{-1})	R^2
PSO				
U(VI)	60.33	60.61	3.83×10^{-3}	1.0000
Th(IV)	59.48	59.88	2.20×10^{-3}	1.0000

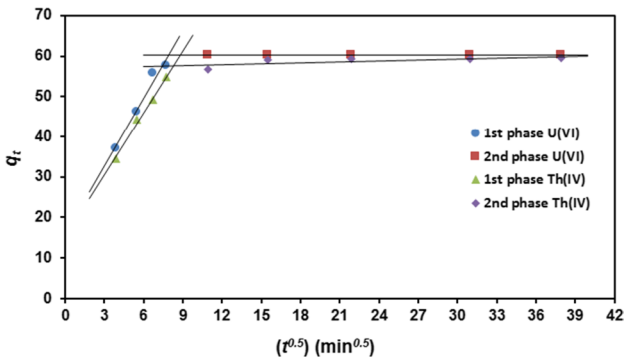

Fig. 9 Intra-particle diffusion plots for U(VI) and Th(IV) ions adsorption onto BSP adsorbent at 25 ± 0.3 °C

Table 6 The calculated Intra-particle parameters for U(VI) and Th(IV) ions adsorption onto BSP adsorbent

Ions	Intra-particle diffusion parameters	
	K_{id}	C
U(VI)	0.40	49.01
Th(IV)	0.50	45.16

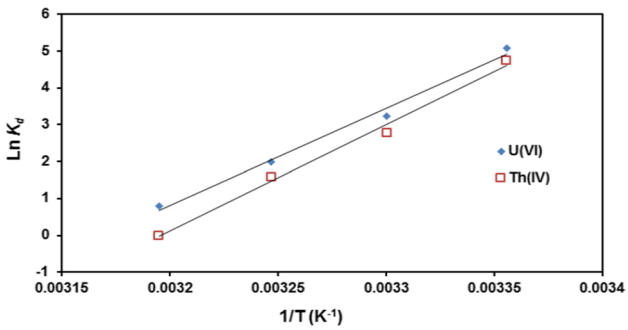

Fig. 10 Plot of ln K_d versus $1/T$ for U(VI) and Th(IV) adsorption onto BSP adsorbent

Conclusion

For the first time a biochar derived from *Salvadora persica* branches was prepared as an efficient adsorbent for U(VI) and Th(IV) ions in water as well as the nature and kinetics of their adsorption onto the prepared BSP adsorbent were studied in this work. The removal efficiency of the BSP biomass adsorbent for U(VI) and Th(IV) reached up to 99% with an adsorption capacity of 85.71 mg g^{-1} and 84.97 mg g^{-1} respectively. The adsorption equilibrium results showed that

Table 7 Thermodynamic parameters for the adsorption of U(VI) and Th(IV)

Temperature (K)	U(VI)			Th(IV)		
	ΔG (kJ mol^{-1})	ΔH (kJ mol^{-1})	ΔS (kJ mol^{-1} K^{-1})	ΔG (kJ mol^{-1})	ΔH (kJ mol^{-1})	ΔS (kJ mol^{-1} K^{-1})
298	− 12.17	− 218.17 ± 15.19	− 0.69 ± 0.05	− 11.45	− 240.17 ± 14.15	− 0.77 ± 0.05
308	− 8.71			− 7.61		
318	− 5.26			− 3.77		
313	− 1.80			0.07		

the adsorption was obtained through a mixed mechanism dominated by chemisorption and followed by pseudo-second-order kinetics. The thermodynamics results revealed that the adsorption of U(VI) and Th(IV) ions onto BSP was spontaneous and thermodynamically favorable with a negative value of ΔG. Also, the adsorption process was exothermic with a negative ΔH. Additionally, the low values of ΔG and the obtained values of ΔH disclose that the adsorption mechanism is mixed and the chemical adsorption is predominant. The negative values of ΔS indicated decrease in randomness at the liquid/solid interface. The findings in this study showed that the biochar derived from *Salvadora persica* (BSP) has a promising performance in water treatment as an adsorbent for uranium and thorium radioactive elements. Therefore, its scaling up and performance in the column bed adsorption system and its reusability will be investigated in another study.

Declarations

Conflict of interest The authors declare that there is no conflict of interest regarding the publication of this article.

References

1. Majdan M, Pikus S, Gajowiak A, Gładysz-Płaska A, Krzyżanowska H, Żuk J, Bujacka M (2010) Characterization of uranium(VI) sorption by organobentonite. Appl Surf Sci 256(17):5416–5421
2. Amit K, Manjoor A, Pandey Badri N (2013) Understanding the biological effects of thorium and developing efficient strategies for its decorporation and mitigation. BARC Newsl 335:55–60
3. Kim JS, Han KS, Kim SJ, Kim S-D, Lee J-Y, Han C, Kumar JR (2016) Synergistic extraction of uranium from Korean black shale ore leach liquors using amine with phosphorous based extractant systems. J Radioanal Nucl Chem 307(2):843–854
4. Bayyari MA, Nazal MK, Khalili FI, Asoudani E (2017) Synergistic effect of tri-n-butyl phosphate (TBP) or tri-n-octyl phosphine oxide (TOPO) with didodecylphosphoric acid (HDDPA) on extraction of uranium(VI) and thorium(IV) ions. J Radioanal Nucl Chem 312(1):133–139
5. Bayyari MA, Nazal MK, Khalili FI (2010) The effect of ionic strength on the extraction of thorium(IV) from perchlorate solution by didodecylphosphoric acid (HDDPA). Arab J Chem 3(2):115–119
6. Bayyari MA, Nazal MK, Khalili FI (2010) The effect of ionic strength on the extraction of Thorium(IV) from nitrate solution by didodecylphosphoric acid (HDDPA). J Saudi Chem Soc 14(3):311–315
7. Anirudhan TS, Rijith S, Tharun AR (2010) Adsorptive removal of thorium(IV) from aqueous solutions using poly(methacrylic acid)-grafted chitosan/bentonite composite matrix: process design and equilibrium studies. Colloids Surf A 368(1–3):13–22
8. Ioannou K, Hadjiyiannis P, Liatsou I et al (2019) U(VI) adsorption by biochar fiber–MnO_2 composites. J Radioanal Nucl Chem 320:425–432. https://doi.org/10.1007/s10967-019-06479-9
9. Liu S, Luo J, Ma J, Li J, Li S, Meng L, Liu S (2020) Removal of uranium from aqueous solutions using aminefunctionalized magnetic platelet large-pore SBA-15. J Nucl Sci Technol. https://doi.org/10.1080/00223131.2020.1796838
10. Soonthornwiphat N, Kobayashi Y, Toda K, Kuroda K, Islam CR, Otake T, Elakneswaran Y, Provis JL, Sato T (2020) Encapsulation of Sr-loaded titanate spent adsorbents in potassium aluminosilicate geopolymer. J Nucl Sci Technol 57(10):1181–1188. https://doi.org/10.1080/00223131.2020.1775717
11. Nazal MK, Al-Bayyari M, Khalili FI (2019) *Salvadora persica* branches biomass adsorbent for removal of uranium(VI) and thorium(IV) from aqueous solution: kinetics and thermodynamics study. J Radioanal Nucl Chem 321:985–996. https://doi.org/10.1007/s10967-019-06668-6
12. Mahramanlioglu M, Bicer IO, Misirli T, Kilislioglu A (2007) Removal of uranium by the adsorbents produced from coffee residues. J Radioanal Nucl Chem 273:621–624
13. Šabanović E, Muhić-Šarac T, Nuhanović M, Memić M (2019) Biosorption of uranium(VI) from aqueous solution by Citrus limon peels: kinetics, equilibrium and batch studies. J Radioanal Nucl Chem 319:425–435. https://doi.org/10.1007/s10967-018-6358-3
14. Öter Ç, Zorer ÖS (2019) Adsorption behaviours of Th(IV) and U(VI) using nitric acid (HNO_3) modified activated carbon: equilibrium, thermodynamic and kinetic studies. Int J Environ Anal Chem. https://doi.org/10.1080/03067319.2019.1691184
15. Halawany HS (2012) A review on miswak (*Salvadora persica*) and its effect on various aspects of oral health. Saudi Dent J 24(2):63–69
16. AG Daful, MR Chandraratne, (2020) Biochar production from biomass waste-derived material. In: Encyclopedia of renewable and sustainable materials, 1st edn, vol 4. Elsevier
17. Tan X, Liu Y, Zeng G, Wang X, Xinjiang H, Yanling G, Yang Z (2015) Application of biochar for the removal of pollutants from aqueous solutions. Chemosphere 125:70–85
18. Langmuir I. (1916). The constitution and fundamental properties of solids and liquids. J Am Chem Soc 38(11): 2221–2295. DOI.https://doi.org/10.1021/ja02242a004
19. Freundlich H (1906) Over the adsorption in solution. J Phys Chem 57(385471):1100–1107

20. Temkin M, Pyzhev V (1940) Kinetics of ammonia synthesis on promoted iron catalysts. Acta Physiochim URSS 12(3):217–222
21. Lagergren S (1898) About the theory of so-called adsorption of soluble substances. Kungliga Sven Vetenskapsakademiens Handl 24:1–39
22. Ho Y, McKay G (1998) A comparison of chemisorption kinetic models applied to pollutant removal on various sorbents. Process Saf Environ Protect 76:332–340
23. Weber W, Asce JM Jr, Morris JC (1963) Kinetic of adsorption on carbon from solutions. J Sanitary Eng Div Proc Am Soc Civ Eng 89:31–59
24. IR-spectrum table and chart. https://www.sigmaaldrich.com/technical-documents/articles/biology/ir-spectrum-table.html. Accessed 26 Sept 2020
25. Fu P, Hu S, Xiang J, Sun L, Yang T, Zhang A, Wang Y, Chen G (2009) Effects of pyrolysis temperature on characteristics of porosity in biomass chars. In: International conference on energy and environment technology, Guilin, October. pp 109–112
26. Suman S, Gautam S (2016) Pyrolysis of coconut husk biomass: analysis of its biochar properties. Energy Sour Part A Recov Util Environ Eff. https://doi.org/10.1080/15567036.2016.1263252
27. Wang J, Hu X, Liu Y, Xie SB, Bao ZL (2010) Biosorption of uranium(VI) by immobilized *Aspergillus fumigatus* beads. J Environ Radioactiv 101(6):504
28. Li F, Li D, Li X, Liao J, Li S, Yang J, Yang Y, Tang J, Liu N (2016) Microorganism-derived carbon microspheres for uranium removal from aqueous solution. Chem Eng J 284:630–639
29. Moulin C, Amekraz B, Hubert S, Moulin V (2001) Study of thorium hydrolysis species by electrosprayionization mass spectrometry. Anal Chim Acta 441:269
30. Lowell S, Shields JE (1991) Powder surface area and porosity, 3rd edn. Chapman and Hall, New Yourk
31. Li L, Quinlivan PA, Knappe DR (2002) Effects of activated carbon surface chemistry and pore structure on the adsorption of organic contaminants from aqueous solution. Carbon 40(12):2085–2100. https://doi.org/10.1016/S0008-6223(02)00069-6
32. Ding D, Xin X, Li L, Hu N, Li G, Wang Y, Fu P (2014) Removal and recovery of U(VI) from low concentration radioactive wastewater by ethylenediamine-modified biomass of *Aspergillus niger*. Water Air Soil Pollut 225:2206–2222
33. Zhang Z, Cao X, Liang P, Liu Y (2013) Adsorption of uranium from aqueous solution using biochar produced by hydrothermal carbonization. J Radioanal Nucl Chem 295:1201–1208
34. Cheira MF, Mira HI, Sakr AK, Mohamed SA (2019) Adsorption of U(VI) from acid solution on a low-cost sorbent: equilibrium, kinetic, and thermodynamic assessments. Nucl Sci Tech 30:156. https://doi.org/10.1007/s41365-019-0674-3
35. Han R, Zou W, Wang Y, Zhu L (2007) Removal of uranium(VI) from aqueous solutions by manganese oxide coated zeolite: discussion of adsorption isotherms and pH effect. J Environ Radioact 93(2007):127–143
36. Tran HH, Roddick FA, O'Donnell JA (1993) Comparison of chromatography and desiccant sillca gels for the adsorption of metal ions-I. Adsorption and kinetics. Water Res 33:2992–3000
37. Rout S, Muduli B, Kumar A, Pulhani V (2020) Removal of uranium(VI) from water using hydroxyapatite coated activated carbon powder nanocomposite. J Environ Sci Health Part A 55(5):596–605. https://doi.org/10.1080/10934529.2020.1721228
38. Morsy A, Taha MH, Saeed M et al (2019) Isothermal, kinetic, and thermodynamic studies for solid-phase extraction of uranium (VI) via hydrazine-impregnated carbon-based material as efficient adsorbent. Nucl Sci Tech 30:167. https://doi.org/10.1007/s41365-019-0686-z
39. BoveiriMonji A, Ghoulipour V, Mallah MH, Maraghe-Mianji B (2015) Selective sorption of thorium(IV) from highly acidic aqueous solutions by rice and wheat bran. J Radioanal Nucl Chem 303:949–958
40. Khalili FI, Al-Banna G (2015) Adsorption of uranium(VI) and thorium(IV) by insolubilized humic acid from Ajloun soil—Jordan. J Environ Radioact 146:16–26
41. Ting C, Nan Z, Zhao X, Xin H, Zhuhong D (2019) Integrated comparisons of thorium(IV) adsorption onto alkali-treated duckweed biomass and duckweed-derived hydrothermal and pyrolytic biochar. Environ Sci Pollut Res 26:2523–2530
42. Hadjittofi L, Pashalidis I (2016) Thorium removal from acidic aqueous solutions by activated biochar derived from cactus fibers. Desalination Water Treat 57(57):27864–27868. https://doi.org/10.1080/19443994.2016.1168580
43. Gado MA, Atia BM, Cheira MF, Abdou AA (2019) Thorium ions adsorption from aqueous solution by amino naphthol sulphonate coupled chitosan. Int J Environ Anal Chem. https://doi.org/10.1080/03067319.2019.1683552
44. Gök M, Sert Ş, Özevci G, Eral M (2018) Efficient adsorption of Th(IV) from aqueous solution by modified SBA-15 mesoporous silica. Nucl Sci Tech 29:95. https://doi.org/10.1007/s41365-018-0432-y
45. Ho Y, McKay G (1999) Pseudo-second order model for sorption processes. Process Biochem 34(5):451–465
46. Pholosi A, Naidoo EB, Ofomaja AE (2020) Intraparticle diffusion of Cr(VI) through biomass and magnetite coated biomass: a comparative kinetic and diffusion study. S Afr J Chem Eng 32:39–55
47. Hu X, Wang J, Liu Y, Li X, Zeng G, Bao Z, Zeng X, Chen A, Long F (2011) Adsorption of chromium (VI) by ethylenediamine-modified cross-linked magnetic chitosan resin: Isotherms, kinetics and thermodynamics. J Hazard Mater 185(1):306–314
48. Saha P, Chowdhury S (2011) Insight into adsorption thermodynamics. In: Tadashi M (ed) Thermodynamics. ISBN: 978–953–307–544–0, InTech, Available from: http://www.intechopen.com/books/thermodynamics/insight-intoadsorption-thermodynamics
49. Zaghouane-Boudiaf H, Boutahala M (2011) Adsorption of 2, 4, 5-trichlorophenol by organo-montmorillonites from aqueous solutions: kinetics and equilibrium studies. Chem Eng J 170:120–126. https://doi.org/10.1016/j.cej.2011.03.039
50. Fendorf SE, Li G (1996) Kinetics of chromate reduction by ferrous iron. Environ Sci Technol 30(5):1614–1617. https://doi.org/10.1021/es950618m